Long-Lived Particles from exotic Higgs decays at the FCC-ee

Magdalena Vande Voorde[1*], Giulia Ripellino[2*†] and Rebeca Gonzalez Suarez[2*†]

[1]Department of Physics, KTH Royal Institute of Technology, Roslagstullbacken 21, 114 21, Stockholm, Sweden.
[2]Department of Physics and Astronomy, Uppsala University, Lägerhyddsvägen 1, 752 37, Uppsala, Sweden.

*Corresponding author(s). E-mail(s): magdalena.vandevoorde@cern.ch; giulia.ripellino@cern.ch; rebeca.gonzalez.suarez@cern.ch;
†These authors contributed equally to this work.

This note presents the first sensitivity analysis for exotic Higgs boson decays at the electron-positron stage of the Future Circular Collider (FCC-ee) within the FCCAnalyses framework. The project studies the production of a Higgs boson in association with a Z boson in electron-positron collisions at a center-of-mass energy of 240 GeV, with the Higgs boson decaying into two long-lived scalars and the Z boson decaying leptonically. A hadronic signature is considered, with the long-lived scalars decaying to a bottom anti-bottom quark pair. Simulations are set up in the FCCAnalyses framework, using MadGraph and Pythia for the event generation and Delphes for the detector simulation. Displaced vertices from the long-lived particle decays are reconstructed based on the FCCAnalyses version of the secondary vertex finding algorithm LCFIPlus, with extended functionality such as custom track selection.

A final event selection requiring the presence of a Z boson and at least two displaced vertices is seen to efficiently remove the Standard Model background, while leaving three or more expected events, including statistical uncertainties, for the majority of the considered parameter space with scalar masses $m_s = 20$ and 60 GeV and mixing angles $\sin\theta = 10^{-5}, 10^{-6}$ and 10^{-7}. The results suggest that the FCC-ee will be sensitive to long-lived scalars with decay lengths of order 1 mm to 10 m, with the peak sensitivity for decay lengths ~ 0.3 m.

1 Introduction

The Standard Model (SM) of particle physics is a consistent theory that has successfully predicted an extensive span of experimental results. Still, there are experimental observations, like the matter anti-matter asymmetry in the Universe and Dark Matter, that the SM cannot explain. To answer some of these open questions new physics beyond the SM (BSM) is needed and several theories have been developed to address the limitations of the SM. Many of these BSM models predict so-called exotic decays of the Higgs boson, i.e Higgs boson decays into new particles [1].

From the present experimental results, no BSM model has yet been confirmed. These null-results have not only resulted in new theories but there have also been further developments experimentally to push the search for new physics beyond the studied regions. One such experimental frontier is the search for long-lived particles (LLPs), which are particles with macroscopic lifetimes. These lifetimes are long enough to give rise to unique detector signals, such as displaced vertices (DVs) [2]. Although motivated in many BSM models, typical searches for BSM physics at colliders assume a prompt decay of the new particle. Hence, through dedicated searches for LLP signatures, new physics can be discovered.

The Future Circular Collider (FCC), is a proposed post-LHC particle accelerator at CERN. It aims to push the energy and intensity frontiers, compared to present and previous colliders, to search for new physics. The FCC is planned to run in two stages, running first as an electron-positron collider (FCC-ee) and then as a hadron collider (FCC-hh).

The overall aim of this project is to investigate exotic Higgs boson decays to LLPs and determine the feasibility to study this model at the FCC-ee. Specifically, the scenario where the LLPs are new long-lived scalar particles is studied. This is the first analysis of its kind conducted within the FCCAnalyses framework. To reach the goal, the project is split into three subsequent studies. First, the long-lived scalar's production and decay process at the FCC-ee is analyzed. Simulated samples of the signal process are generated and validated compared to theoretical predictions. The second study focuses on the detector response and reconstructed observables related to the signal signature. As the signal consists of unconventional DVs, standard reconstruction algorithms and identification techniques cannot be utilized directly and must be adapted. Finally, an event selection is applied to assess the sensitivity of the signal.

The note is based on the master thesis "Long-Lived Particles from exotic Higgs decays at the FCC-ee" [3] and the structure of the note is as follows. First, exotic Higgs boson decays and the BSM model generating the long-lived scalars are introduced in Section 2. Secondly, Section 3 presents the FCC-ee. Furthermore, the simulation tools are presented in Section 4, while the reconstruction methods within the FCCAnalyses framework, as well as the developed method to reconstruct DVs, are outlined in Section 5. In Sections 6 to 8, the main results and discussions of this project are presented. The first step of generating and validating simulation samples is discussed in Section 6, while Section 7 presents an analysis of the reconstructed observables. Finally, the event selection and the sensitivity analysis are presented along with a related discussion in Section 8.

2 Exotic Higgs boson decays

The decay width of the Higgs boson is tiny in comparison with its mass, and current bounds from the measurements of the total width provide large possibilities for interactions with BSM particles. These can result in so-called exotic decays, i.e decays into new light BSM particles. There are many BSM models that give rise to exotic Higgs decays, such as the two-Higgs-doublet models, Little Higgs models, Next-to-Minimal Supersymmetric Standard Model, and Hidden Valleys models, all providing answers to several different open questions [1].

The Hidden Valley model introduces an extended sector of light-state particles interacting weakly with the SM via a heavy mediator [4]. These models are motivated for instance by models of neutral naturalness, where neutral naturalness address the hierarchy problem of the SM [5]. Since this potentially new sector of particles only interacts weakly with the SM it is referred to as the hidden or dark sector. Some frameworks providing answers to Dark Matter are other examples of models where a hidden sector is introduced [6]. The heavy mediator is often referred to as the portal since it is the link between the SM and the hidden sector. In several of these models, the portal is a new scalar particle coupled to the Higgs boson, and it is possible for this new scalar to be long-lived. A comprehensive study of exotic Higgs boson decays with related theoretical models and possible experimental signatures are provided in the review [1]. For a more recent review, including results for LLPs searches, see [7].

2.1 A scalar extension of the Standard Model

A general model that establishes the scalar particle introduced in the previous section is an extension of the SM by an additional real single scalar field. This extension of the SM is achieved by a scalar field S that interacts with the Higgs field doublet H via the portal term $\frac{1}{2}\kappa S^2|H|^2$, governed by the coupling constant κ. The minimal renormalizable Lagrangian is then [7],

$$\mathcal{L}_{SM} \ni \underbrace{\frac{1}{2}\mu_S^2 S^2 - \frac{1}{4!}\lambda_s S^4}_{\text{scalar potential}} - \underbrace{\frac{1}{2}\kappa S^2 |H|^2}_{\text{portal term}}$$

where the two last terms are the Higgs potential of the SM with its couplings μ and λ, and the two first terms are the scalar potential determined from the scalar mass-term μ_S and the self-interaction coupling λ_S. The Lagrangian is also subject to a forced discrete Z_2 symmetry such that the Lagrangian is invariant under the exchange of signs of S, i.e $S \to -S$, which removes linear and cubic terms of S. Depending on the values of μ_S and λ_S the scalar field will, just like the Higgs field, require a non-zero vacuum expectation value, v_s. Consequently, the scalar and the SM Higgs can mix into physical particle states that may decay into SM particles.

The partial decay width of the Higgs boson to the new scalars is given by [7],

$$\Gamma(h \to ss) \approx \frac{\kappa^2 v_h^2}{32\pi m_h}\sqrt{1 - 4\frac{m_s^2}{m_h^2}}, \tag{1}$$

where $v_h = 246$ GeV is the usual Higgs vacuum expectation value, $m_h = 125$ GeV is the observed Higgs boson mass and m_s is the physical mass of the scalar particle. The decay of the scalar is determined by its partial decay width which is given at leading order by [1],

$$\Gamma(s \to f\bar{f}) \approx \sin^2\theta \frac{N_c}{8\pi} \frac{m_s m_f^2}{v_h^2} \left(1 - \frac{4m_f^2}{m_s^2}\right)^{3/2}, \tag{2}$$

where m_f is the mass of the decay product fermion, N_c is the number of colors. i.e equaling 3 for quarks and 1 for leptons, and $\sin\theta$ is the so-called mixing angle. From Equations (1) and (2) the branching ratios $BR(s \to \mathrm{SM})$ and $BR(h \to ss \to \mathrm{SM})$ can be computed and are shown in Figure 1. The mixing angle is the main coupling determining the lifetime of the scalar s. For sufficiently small values the lifetime is macroscopic, e.g $c\tau \sim$ meters when $\sin\theta \leq 10^{-6}$ [1], yielding exotic Higgs boson decays to pairs of long-lived scalars.

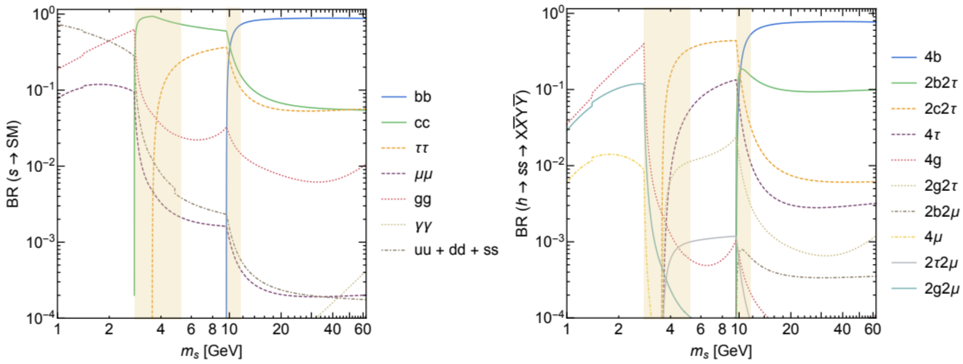

Fig. 1: Two branching ratios BRs as a function of the scalar mass m_s. To the left, for the scalar to different SM particles, and to the right for the full process of exotic Higgs decays. In the right plot, the branching ratio is scaled to $BR(h \to ss) = 1$. Image is taken from [1].

In summary, there are two main processes and couplings in this model that are of importance to study the exotic Higgs decays into long-lived scalars. First, pair production of the scalar s via the Higgs boson decay, governed by the coupling κ. Secondly, the lifetime of the scalar and its decay into the SM particles, governed by the mixing angle $\sin\theta$.

2.2 Current constraints and possible future sensitivity

Searches for exotic Higgs boson decays into long-lived scalars, with different SM decays, are being conducted at various experiments. From current results, no scalar has been discovered, and 95% CL exclusion limits on the branching ratio $BR(h \to ss)$ have been set. These limits are summarized in Figure 2 for mean proper lifetimes in the span of 0.1 mm to 10 m, with scalar mass m_s = 30-40 GeV. In the figure, the lines represent different searches conducted by the experiments ATLAS, CMS, and LHCb. These searches cover different final state particles as well as different LLP signatures. The investigated LLP signatures in these searches are large impact-parameter tracks and (DVs) reconstructed in the inner tracking detector (ID), displaced hadronic jets or photons in the calorimeter, and displaced signals from jets or leptons in the muon system (MS) [7].

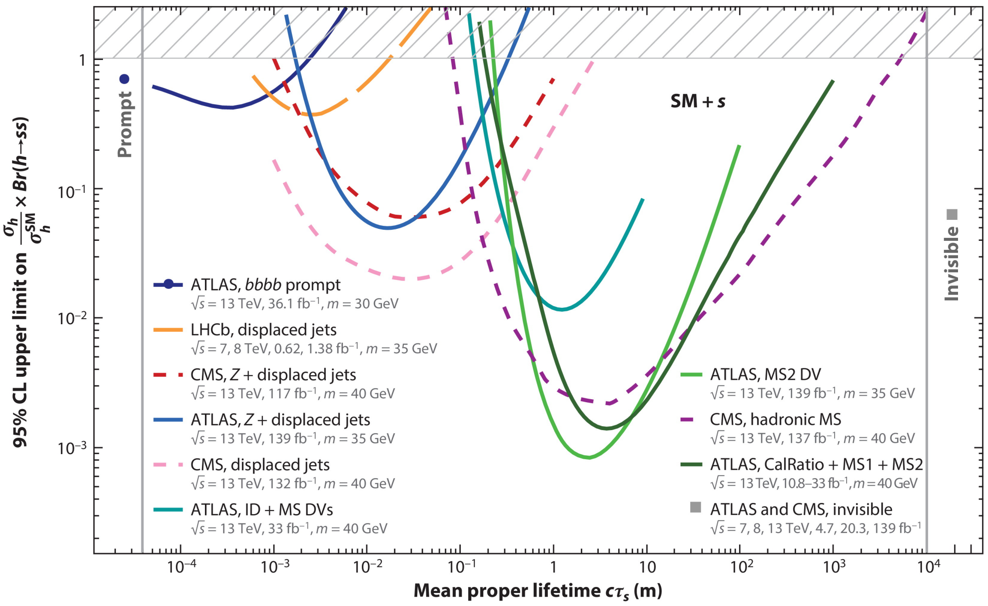

Cepeda M, et al. 2022
Annu. Rev. Nucl. Part. Sci. 72:119–49

Fig. 2: Observed 95% CL upper limits on the $BR(h \to ss)$ in the extended SM with a scalar, in the scenario where s is long-lived and decaying hadronically. The exclusion limits are set from searches done at LHC by the different experiments ATLAS, CMS, and LHCb considering different LLP signatures. Image is taken from [7].

Future experiments have the possibility to probe the model even further and search for long-lived scalars with higher sensitivity. A previous study [8] investigated the potential sensitivity for LLPs from exotic Higgs boson decays at the proposed future collider FCC-ee. The FCC-ee is presented in detail in the next Section 3. Results suggest a peak sensitivity of BR$(h \to ss) \sim 5 \times 10^{-5}$ (projected 95% CL upper limit) for scalar masses in the range from 2.5 to 50 GeV with decay lengths between 0.01 mm to 10 m. This can be translated to a lower limit on the coupling $\kappa \sim 10^{-4} - 10^{-4}$ and a limit on the range for the mixing angle, from $\sin\theta \sim 10^{-7}$ to 10^{-4}, for a scalar mass of 50 GeV [8].

3 The Future Circular Collider

The Future Circular Collider (FCC) project is a proposed new particle accelerator located at CERN in Geneva, Switzerland. A schematic figure of the accelerator and its placement is shown in Figure 3. For size comparison, the LHC is also shown. The FCC will have a circumference of around 90 km, compared to the LHC circumference of 27 km. An integrated program has been proposed by the FCC project. At first, the FCC is suggested to operate as a high-luminosity electron positron collider, the FCC-ee, and then as a hadron collider, the FCC-hh. This is in line with the LHC program which was precedented by the LEP collider operating in the same tunnel but with beams of electrons and positrons. The aim of the FCC-ee is to achieve precise measurements of the properties of W and Z bosons, the top quark and the Higgs boson, while the FCC-hh will push the energy frontier reaching a collision energy of 100 TeV and directly search for new phenomena. Thus, the full FCC program has a great possibility to explore and extend the current knowledge of the SM [9].

The FCC was proposed by CERN as a response to the European Strategy for Particle Physics (ESPPU) in 2013. A design study was carried out in 2014-2020, resulting in the Conceptual Design Reports in which a feasibility study was requested [9]. The feasibility study is currently ongoing and will be presented at the next ESPPU meeting in 2025. If the project is approved before the end of this decade, construction can start in the early 2030s and the FCC-ee can start running in 2045 and operate for 15 years. The FCC-hh will then operate for 25+ years.

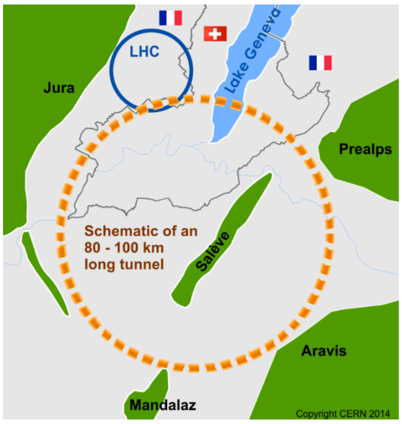

Fig. 3: Schematic figure of the FCC ring, marked with a dashed orange line, and its placement at CERN. Image is taken from [10].

3.1 Physics motivation for the FCC-ee

The FCC-ee is proposed to run in several stages at energies ranging from 90 to 365 GeV. Compared to the LEP collider, the magnitude of the predicted increase in integrated luminosity for the FCC-ee is as big as 10^5 at the energy of 90 GeV [11]. The current estimated production of the collider at the different stages is 6 $\times 10^{12}$ Z bosons at 91 GeV, 2.4 $\times 10^{8}$ W boson pairs at 160 GeV, 1.45 $\times 10^{6}$ Higgs bosons at 240 GeV and 1.9 $\times 10^{6}$ $t\bar{t}$ pairs at 350 GeV. The high statistics will significantly increase the precision by which the properties of these particles can be studied compared to present analyses. Constraining the parameters could reveal deviations from the SM predictions, which in turn hints at new physics at higher energies than those currently reachable [9].

Although the primary physics motivation for the FCC-ee is the precision measurements of the Higgs, W and Z bosons, and the top quark, the high statistics of these particles and the clean experimental signature compared to hadron collisions are also important to directly observe BSM physics and new phenomena. In particular, BSM theories including new particles with small couplings to the SM can be probed. Such particles could then manifest as LLPs. Three LLP physics cases with discovery potential at FCC-ee are Heavy Neutral Leptons (HNLs), Axion Like Particles (ALPs) and various exotic Higgs decays to LLPs [11].

3.2 The International Detector for Electron-positron Accelerators

There are mainly two detector designs proposed for the FCC-ee, the International Detector for Electron-positron Accelerators (IDEA) [12] and the CLIC-Like Detector (CLD) [13]. Both designs are based on the detectors of previous and present colliders with further developments based on years of research in the sector, and optimized for the FCC-ee conditions [11]. This project uses the IDEA design for the detector simulations.

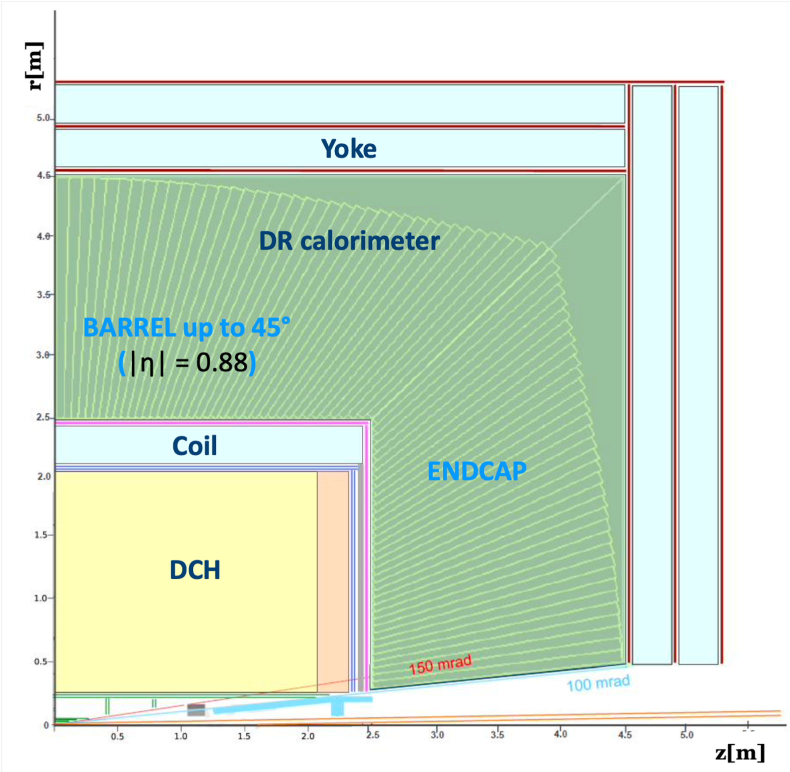

Fig. 4: The current layout of IDEA that illustrates the different parts and their position along the beamline in the z-direction and the radius r of the transverse plane. Image is taken from [14].

A schematic picture of the IDEA detector is shown in Figure 4, highlighting the different parts and subdetectors. Further details of each part are given below.

Silicon pixel vertex detector: A high-granularity tracking detector, designed to precisely reconstruct the vertices close to the collision point. The beam-pipe has a radius of $\sim$ 1 cm, and the vertex detector has an inner part with three layers of silicon detectors between 1.2 cm and 3.15 cm and an outer part which extends up to 34 cm.

Drift Chamber (DCH): An additional tracking system, designed for high precision momentum measurements and good particle identification. It is placed outside the vertex detector with a radius extending from 35 to 200 cm. The DCH is surrounded by a layer of a silicon detector, for precise space point measurement, and a superconducting solenoid coil, to bend the trajectories of the charged particles. The coil extends from a radius of 2.1 to 2.4 m.

The Dual-Readout (DR) calorimeter: A calorimeter designed to measure both hadronic and electromagnetic energy deposits. It is sensitive to both scintillation light produced mainly by hadrons and Cherenkov light mainly from relativistic electrons (the electromagnetic component). Hence separate measurements of the two different energy deposits can be done. The DR calorimeter is 2 m and extends from a radius of 2.5 to 4.5 m

Muon chamber: The last subdetector designed to detect muons. The chamber is embedded in a 1 m wide magnetic return yoke. The muon system extends out to a radius of 5.5 m which thus corresponds to the full IDEA detector radius.

The IDEA detector concept is still under investigation for further optimization. To optimize the detector for LLP searches timing capability and vertex resolution are important factors.

4 Simulation and Software Setup with FCCAnalyses

Simulations of collision processes and detector environments are a key component in particle physics research, both for BSM searches and precision studies. The simulated data based on the theoretical predictions lays the foundation for the hypothesis to be confirmed or rejected by observed data from the experiments. In terms of feasibility studies, simulations are vital to precisely simulate the particle kinematics and the detector response, both to analyze the prospective sensitivity of the signal as well as guide in defining the detector design.

This study is set up in the FCCAnalyses framework. Simulations are done using the software tools `MadGraph` [15], PYTHIA [16] and DELPHES [17] with output in the EDM4HEP format. The eventual analysis is scripted in Python, and mainly based on the class RDataFrame of the data analysis framework ROOT. The common analysis workflow in the FCCAnalyses framework is split into different files in three stages. The first stage runs on the generated simulation samples and returns the key variables to be studied. The second stage determines the event selection and specifies variables to be plotted in histograms, which happens in the last stage. The rest of this section is dedicated to describing the simulation tools in further detail.

4.1 Simulation with MadGraph, Pythia and Delphes

An e^-e^+ collision event is a complex process involving several multi-particle interactions. Hence, for simulations, the structure of an event can be split into different levels and calculations. First is the hard scatter process of the e^- and e^+ collision, which is followed by parton showering and hadronization to describe the final state, and finally the detector response to mimic how the event looks like in the collider. To compute these calculations Monte Carlo (MC) generators are used, which are algorithms based on the MC method of repeated random sampling to get a numerical solution.

In the hard scatter process, the cross section and kinematical properties are computed for the considered signal process. From the e^-e^+ collision to the N particle final state. At this stage, colored charged particles such as quarks, anti-quarks and gluons, are treated as free particles. This project uses `MadGraph` for these calculations. `MadGraph` is an MC generator commonly used to perform SM and BSM simulations and generate events. It computes the cross sections at leading order as well as next-to-leading order, where higher order terms are included to increase the precision [15].

The interacting electron and positron may emit radiation before and after the hard scatter, resulting in initial and final state radiation. This is simulated with a so-called parton shower algorithm. At last, since free colored charged particles do not exist, every final state quark or gluon, both from the hard scattering process and the parton shower, must end up in a hadron. This is called hadronization. To perform this step on the events generated by `MadGraph`, this project uses PYTHIA. Just like `MadGraph`, PYTHIA generates events from the hard scatter process but it also includes simulation of parton shower, hadronization, and other strong interaction phenomena [16].

The last part of the simulation chain lets the final state particles of the generated events move through a model of the detector geometry and material, and simulate the response. This project uses an IDEA model in the simulation framework DELPHES for a so-called fast parametric detector simulation. In a parametrized simulation the overall detector response is simulated in a parametric way, therefore the particles are assigned values that are dependent on their location in the detector. While in a full simulation, the particles are propagated through the detector material step-by-step and the response at each point is calculated from e.g the Bethe-Bloch formula, to include all physical effects. The DELPHES fast simulation includes a tracking system in a magnetic field, calorimeters, and a muon system. Some output observables are leptons, missing transverse energy and jets [17].

5 Object Reconstruction, Tracking, and Vertexing

The output from the IDEA Delphes simulation has to be reconstructed into meaningful physics objects such as muons, electrons and photons, and other objects as missing transverse energy, jets, and tracks. Another important part of event reconstruction is vertex reconstruction, where tracks are fitted to their corresponding decay vertex which they originate from. In the following section, the tracks, the vertex fitting algorithm and the primary vertex finding are presented in more detail, followed by a description of the secondary vertex finding algorithm and the reconstruction of DVs.

5.1 Tracks

The trajectory of a charged particle in a magnetic field can be described by a helical path with five parameters. In FCCAnalyses the tracks are thus described by a set of five parameters and a 5 × 5 covariance matrix, including the uncertainties of each measured parameter and their correlations. Using the canonical representation with respect to the collision point the parameters and the corresponding uncertainties can be calculated given that a point on the track, its momentum at the point, and its charge are known. The five parameters are,

$$t_{\text{param}} = (d_0, \rho_0, z_0, \tan\lambda, \phi),$$

where d_0 and z_0 are the transverse and longitudinal impact parameters, i.e the distance of the closest approach to the interaction point in the transverse, or longitudinal, plane. The others are ρ_0, which describes the curvature of the track, the azimuthal angle ϕ at the closest approach, and tan λ, which is related to the polar angle θ of the track, where $\lambda = \cot\theta$.

5.2 Vertex fitting

A vertex is reconstructed with an algorithm that takes a set of tracks and finds a common intersection point and its uncertainties in the (x, y, z) space. The fitting is done given that the set of tracks originated from the same single vertex. The vertex fitting algorithm (vertex fitter) includes the following three steps:

1. Start with tracks expressed with respect to an initial vertex position hypothesis, e.g the beam spot or the detector origin
2. Vary the track parameters within their respective uncertainties
3. Find a common intersection point with the minimal value of the goodness-of-fit measure χ^2

To find the set of tracks likely originating from the same vertex, a vertex finder algorithm is used.

5.3 Primary vertex finder

At the LHC several primary vertices are reconstructed in each bunch crossing event, where the vertex with the highest momentum is the PV and the rest of the vertices are so-called pile-up. For the FCC-ee a low pile-up rate is predicted [18], hence, there will be a maximum of one reconstructed PV in each event. A main goal of a PV finding algorithm (PV finder) is to separate tracks originating from the PV and tracks originating from other vertices, e.g SVs. The PV finder includes the following steps:

1. Set the initial vertex position hypothesis to be the beam spot, typically $x = 4.5\mu$m, $y = 20$ nm and $z = 0.3$ mm in FCC-ee simulations, use the vertex fitter with all the tracks in the event
2. From the initial set of tracks, remove the track with the highest contribution to the χ^2 fit of the vertex, refit and repeat this step until there is no track left with a contribution higher than 25; these are the primary tracks

5.4 Secondary vertex finder

The decay vertices of the B and C hadrons are usually referred to as SVs because of their displaced distance from the collision point, and detectors are usually designed to reconstruct them with high precision. Finding the SVs is a crucial step in determining the flavor of heavy hadrons jets. The LCFIPlus framework [19] implements several tools for jet flavor identification, including a secondary vertex finding algorithm (SV finder), developed for future linear e^+e^- colliders. The SV finder implemented in FCCAnalyses is based on the LCFIPlus framework's vertex finding, using the vertex fitter presented in the previous Section 5.2, and is summarized in the following steps:

1. Form all possible pairs with the non-primary tracks and fit these to vertex candidates with the vertex fitter. To find the vertex seed out of the vertex candidates they are filtered by following constraints:

- V^0 rejection[1], meaning the vertices and tracks stemming from a V^0 particle (K^0_S, Λ^0 or γ_{conv}) are removed
- The χ^2 of the vertex must be less than a threshold (standard input is 9)
- The invariant mass M_{inv} of the vertex must be less than a set upper limit (standard input is 10 GeV)
- The direction of the distance from the PV to the vertex must be on the same side as the direction of the sum of the momenta from both tracks

2. Of all vertices passing the criteria, the one with the lowest χ^2 contribution is chosen as the vertex seed
3. Iteratively, additional tracks are added to the vertex seed if the χ^2 contribution is less than a set upper limit (standard input is 5)
4. Remove the tracks belonging to the vertex from the initial set of secondary tracks and repeat step 2 and 3 until all vertices are found

5.5 Reconstruction of displaced vertices

This section presents the procedure for DV reconstruction. It is mainly based on the SV finder presented in Section 5.4, using all the standard inputs of the threshold values except the invariant mass at the vertex which is increased to $M_{inv} = 40$ GeV. Additionally custom track selection and vertex merging were implemented to target the DV, these methods are described in further details in the following subsections. The applied cuts for the custom track selection and the criteria for vertex merging are the same criteria used for the DV reconstruction algorithm in the ATLAS collaboration [20]. For further studies optimization for FCC-ee should be carried out. The full reconstruction scheme is summarized in Algorithm 1.

5.5.1 Track selection

In order to adapt the SV finder to the reconstruction of DVs, a selection was developed for the tracks used as input to the algorithm. The tracks are required to have a transverse momentum $p_T > 1$ GeV, such that they are of high quality. Moreover, all tracks are required to have a transverse impact parameter $|d_0| > 2$ mm. This is applied since the long-lived scalars have large values of the d_0, due to their long decay path.

5.5.2 Vertex merging

Applying the custom track selection several DVs belonging to each long-lived scalar decay can be reconstructed. Particularly considering a final state of b quarks, since the large mass of the b quarks relative to the lighter quarks results in a decay chain of $b \to c \to s \to d$ from which several vertices are formed. This can lead to a high multiplicity of reconstructed vertices which in turn leads to a degradation in measured quantities like the invariant mass. Since the invariant mass is predicted to be a good variable to discriminate a DV stemming from the LLP with a DV from a SM process or a fake vertex, it is crucial to be as accurate as possible. Reconstructed vertices are

[1] The V0 particles are identified based on kinematic variables like the reconstructed mass and the angle and the distance of the V0 vertex with respect to the PV. The selection cuts put on these variables are summarized in Table 1 of the LCFIPlus framework paper [19]

compared pair-wise and if the distance between their positions is less than 10 times the error of the distance or 1mm, they are merged. The merged vertices are refit with all the tracks associated with the two initial vertices.

Algorithm 1 Reconstruction of Displaced Vertices

```
Stage one: Fit the PV
From the fit, separate between primary and secondary tracks
Stage two: Find the DVs
Select secondary tracks with p_T > 1 GeV and |d_0| > 2 mm
Use the selected tracks in the SV finder, with input parameters: χ^2 of vertex < 9,
M_inv < 40 GeV, and χ^2 contribution < 5
Stage three: Merge nearby vertices
Compare the vertices pair-wise by computing the distance between them and the
error of the distance, σ
if The distance between the positions is < 10σ or < 1 mm then
    Take the associated tracks of the considered vertices, combine and rerun the
    vertex fitter
end if
```

6 Simulation of Long-Lived Scalars from exotic Higgs decays

To study long-lived scalars from exotic Higgs decays at FCC-ee a specific production and decay process of the particle is chosen for the analysis and is referred to as the signal. This section introduces the signal process, the specific parameter space that is scanned, and how the simulations are generated. The section also includes validations of the signal samples by comparing the simulated data with theoretical predictions.

6.1 Production and decay at FCC-ee

The specific signal process considered in this thesis is $h \to ss \to b\bar{b}b\bar{b}$, i.e the Higgs decaying into two scalars which in turn decay into two b-quarks each. The b-quark final state is chosen since it is the dominant decay channel, for a scalar mass above 10 GeV, see Figure 1. At the FCC-ee the Higgs boson is predominantly produced together with a Z boson at a center-of-mass energy of $\sqrt{s} = 240$ GeV. In the simulation the Z boson is decayed into an electron or muon pair according to $Z \to e^+e^-$ or $\mu^+\mu^-$. Hence, the complete production process of the signal at the FCC-ee is,

$$e^+e^- \to Zh \text{ with } Z \to e^+e^- \text{ or } \mu^+\mu^- \text{ and } h \to ss \to b\bar{b}b\bar{b}, \tag{3}$$

which is illustrated with a Feynman diagram seen in Figure 5.

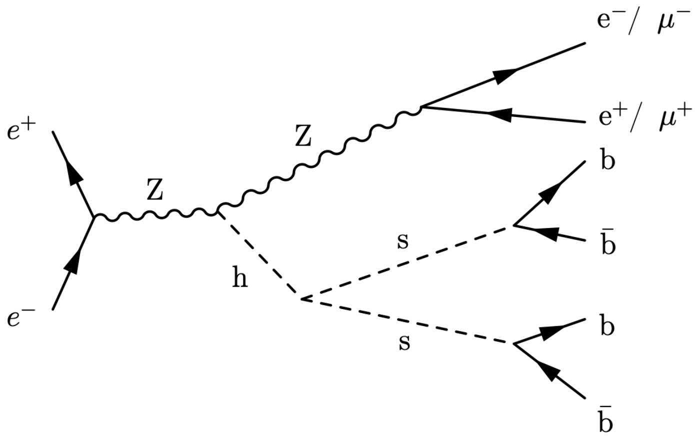

Fig. 5: Feynman diagram of the complete process of the signal $h \to ss \to b\bar{b}b\bar{b}$ produced at the FCC-ee from $e^+e^- \to Zh$ with the Z boson decaying into e^+e^- or $\mu^+\mu^-$-pairs.

.

6.2 Simulating the signal process

To generate the signal process in Equation (3) in `MadGraph` the HAHM_MG5Model_v3 [1, 21] is used. This corresponds to the Hidden Abelian Higgs Model (HAHM) which in addition to the scalar contains another BSM particle, a vector referred to as the dark photon. The HAHM_MG5Model_v3 has four input parameters; the mass of the dark photon, m_{ZD}, the kinetic mixing coupling constant of the dark photon, ϵ, the mass of the scalar, m_s and the coupling constant between the scalar and the Higgs boson, κ. To only consider the SM + scalar case with this model the dark photon is decoupled by setting a high mass, $m_{ZD} = 1000$ GeV, and a low coupling, $\epsilon = 10^{-10}$.

To generate long-lived scalars, in addition to the input parameters, the width of the scalar is set in the process card of `MadGraph`. The total decay width of the scalar for a $b\bar{b}$ final state can be calculated as [1],

$$\Gamma_s = \sin^2\theta \frac{3}{0.9 \times 8\pi} \frac{m_s m_b^2}{v_h^2} \left(1 - \frac{4m_b^2}{m_s^2}\right)^{3/2} \tag{4}$$

where the branching ratio $BR(s \to b\bar{b})$ equals 0.9, as seen in the left plot in Figure 1, and the expression for the partial decay width at leading order was given in Equation (2). Furthermore, the b quark mass is $m_b = 4.2$ GeV, the Higgs vev $v_h = 246$ GeV and the number of colors $N_c = 3$. By setting the width of the scalar by hand in the `MadGraph` process card the lifetime of the scalar can be properly controlled.

All signal samples are generated with 10.000 events. The generated scalar masses and mixing angles, with the corresponding width, are summarized in Table 1. The considered masses are $m_s = 20$ GeV and $m_s = 60$ GeV, covering two ends of the allowed parameter space for a scalar decaying to $b\bar{b}$ quarks. The mixing angles are sinθ = $10^{-5}, 10^{-6}$ or 10^{-7} for each mass, corresponding to decay lengths of order 1 mm to 10 m. The scalar-Higgs coupling constant κ is set to $\kappa = 0.0007$ for all signal samples, such that the order of the branching ratio is $BR(h \to ss) \propto 10^{-4}$. This is lower than current constraints from searches at LHC, and has been shown to be within reach for FCC-ee from previous studies [8], see Section 2.2.

Table 1: Generated values for the scalar mass m_s and mixing angle sin θ, with corresponding scalar width Γ_s and mean proper lifetime $c\tau$.

Mass of Scalar m_S [GeV]	Mixing angle sin θ	Width of Scalar Γ_s [GeV]	Mean proper lifetime $c\tau$ [mm]
20	1×10^{-5}	5.779×10^{-14}	3.4
20	1×10^{-6}	5.779×10^{-16}	341.7
20	1×10^{-7}	5.779×10^{-18}	34167.0
60	1×10^{-5}	2.252×10^{-13}	0.9
60	1×10^{-6}	2.252×10^{-15}	87.7
60	1×10^{-7}	2.252×10^{-17}	8769.1

The signal processes are generated step-by-step in a simulation chain with `MadGraph` [15] v.3.4.1 for MC generation, PYTHIA [16] v.8303 for parton showering and hadronisation, and DELPHES [17] v. 3.4.2 with the spring2021 IDEA card for detector simulation. Six signal samples are generated with the parameters specified in Table 1.

6.3 Validation of generated quantities

Validation of the signal samples was carried out by studying some generated variables at truth-level, i.e studying the particle kinematics before the simulation of the detector effects. Emphasis was put on the decay lengths and time distributions of the long-lived scalars.

In most of the following histograms, there is a general labeling. Starting at the top left corner the first row states the center-of-mass energy, $\sqrt{s} = 240$ GeV and the next row specifies the luminosity $L = 7.2\text{ab}^{-1}$. Furthermore, the third row shows the signal process given in Equation (3), and the last row specifies that no selection has been made on the events. In the legend, the different signal samples are titled after their mass, m_s, and mixing angle, sin θ. The x-axis shows the considered variable and the y-axis indicates in log scale the number of events per bin width. The number of events has been scaled to their cross section, see Table 8, and luminosity. Finally, the title of the plot specifies that simulations are done for FCC-ee with Delphes, in the FCCAnalyses framework.

6.3.1 Generated decay lengths

In order to validate the simulation of the long lifetime the decay lengths L_{xyz} of the scalars are studied. This corresponds to the distance traveled by the scalar before decaying to the $b\bar{b}$-pair, as measured in the lab frame. This is given by,

$$L_{xyz}^{truth} = \sqrt{\Delta x^2 + \Delta y^2 + \Delta z^2},$$

where $\Delta x, y, z$ are the differences between the production vertex of s and the production vertex of the $b\bar{b}$-pairs in terms of the x, y, z coordinates.

The decay lengths for all signal samples are plotted in Figure 6. The x-axis has the range of 0-2000 mm, i.e from the collision point of the e^+e^- beams to the outer radius of the drift chamber of IDEA $R_{out} = 2$ m, see Figure 4. The signal samples with mixing angle $\sin\theta$ = 1e-7, both for $m_s = 20$ GeV (green) and $m_s = 60$ GeV (light purple), over 99% of the decay lenths are in the overflow. The scalar might therefore be too long-lived to be properly reconstructed within the DCH of IDEA.

For mixing angle $\sin\theta$ = 1e-6, the heavier mass sample with $m_s = 60$ GeV (orange) has a shorter decay length than the sample with $m_s = 20$ GeV (blue). This follows the expected behavior since the width of a particle is determined both from the matrix element and the phase space factor. Hence for the same coupling, a heavier scalar mass corresponds to a larger decay width, resulting in a shorter decay length.

Finally, the general dependence of the decay length on the mixing angle can be confirmed by comparing the signal samples with the same mass. Within each group, the decay length increases as the mixing angle decreases, in agreement with Equation (4).

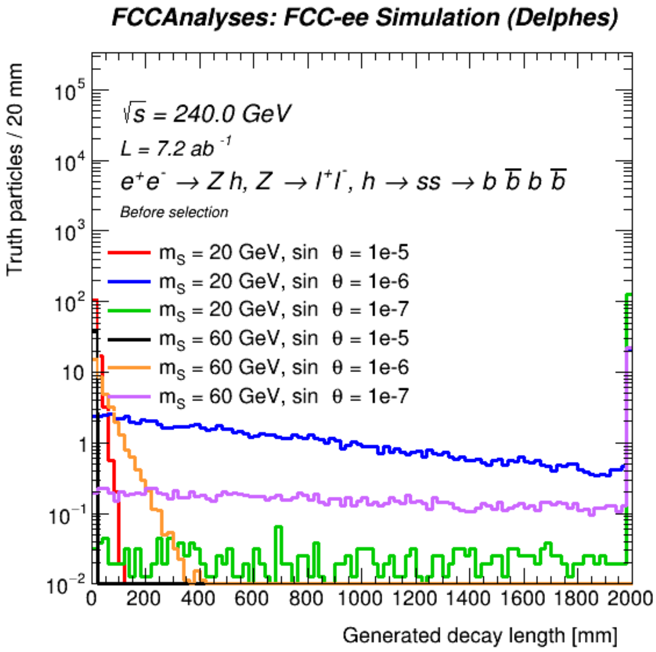

Fig. 6: Generated decay lengths, L_{xyz}^{gen}, for all signal samples

.

6.3.2 Generated time distributions

The lifetime distributions are further investigated in the reference frame of the scalar. Since the measured decay length L_{xyz} can be rewritten as $L_{xyz} = ct_{lab}$, the proper lifetime τ can be calculated as,

$$\tau = \frac{L_{xyz}}{c\gamma},$$

where $\gamma = \frac{E_s}{m_s}$. Figure 7 shows the lifetime distribution of the scalars for the $m_s =$ 20 GeV (7a) and $m_s = 60$ GeV (7b) samples. These distributions follow the expected behavior with a longer lifetime for a smaller mixing angle. As already shown for the decay lengths, the same mixing angle corresponds to a shorter lifetime for the higher mass. In Figure 7 this is most visible for sin $\theta =$ 1e-6, where the end of the time distribution for $m_s =$ 20 GeV (blue) extends to 8 ns while it ends around 1 ns for $m_s =$ 60 GeV (orange).

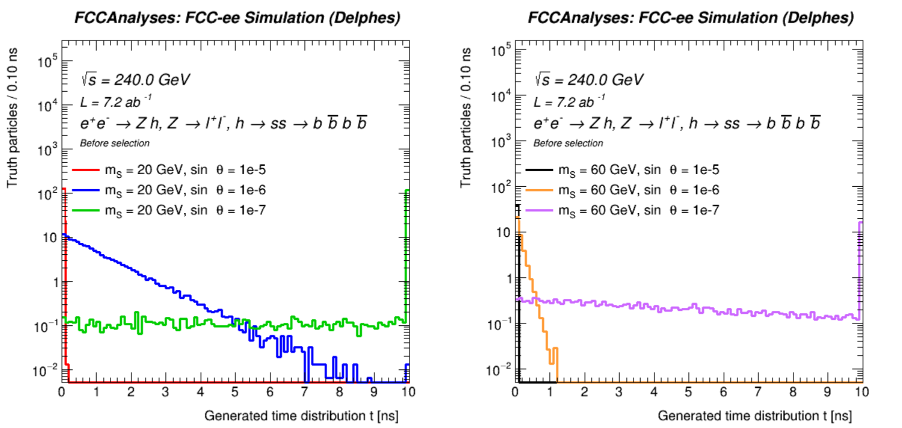

(a) $m_s =$ 20 GeV, sin $\theta =$ 1e-5, 1e-6, 1e-7 (b) $m_s =$ 60 GeV, sin $\theta =$ 1e-5, 1e-6, 1e-7

Fig. 7: Distribution of the lifetimes for all signal samples.

For further validation of the simulation, the mean proper lifetime from the simulations is compared to the calculated value. The lifetime distribution is fit to an exponential function, in order to extract the mean proper lifetime τ_0.

The theoretical proper mean lifetime can be calculated from the decay width of the scalar which is computed according to Equation (4). In Figure 8, the time distributions for the signal samples with $m_s =$ 20 GeV are plotted separately for each considered mixing angle. The generated lifetimes are plotted in blue, and the exponential fit in red. The τ_0 from the fit is shown together with the result from the calculations in the legend.

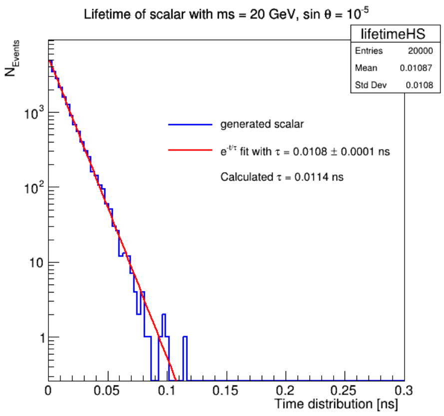

(a) sin θ = 1e-5

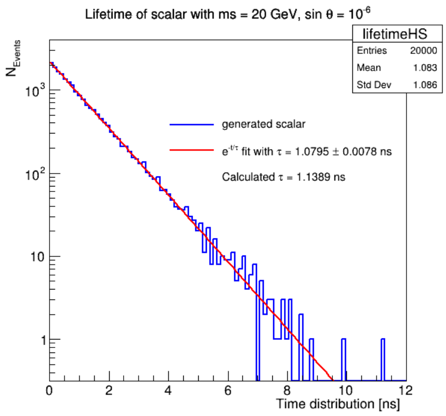

(b) sin θ = 1e-6

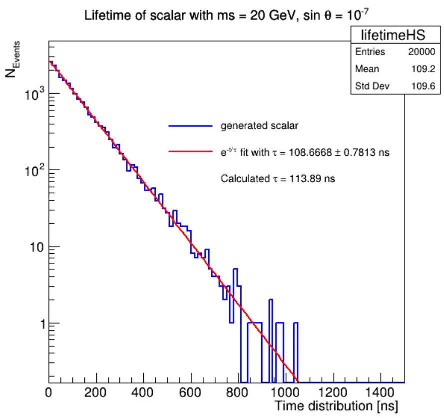

(c) sin θ = 1e-7

Fig. 8: Time distributions with exponential fit for each mixing angle sin θ = 1e-5, 1e-6 and 1e-7 with mass m_s = 20 GeV. Note, this figure does not follow the general labeling. The y-axis is not scaled to the cross section and luminosity but shows the number of generated events. Additionally, the extra box in the top right corner of each histogram plot shows the number of entries, i.e the number of events, the mean value, and the standard deviation of the histogram.

In all three cases, the generated value is lower than the calculated value, also when considering the statistical error. Still, the theoretical calculations and the fit values do not differ more than 5.2%. Hence, including the previous results, it is concluded that the signal samples are valid for this analysis.

7 Analysis of Reconstructed Quantities

7.1 Reconstructed Z from e^+e^- or $\mu^+\mu^-$

The signal process considered for this study restricts the Z boson decays to either e^+e^- or $\mu^+\mu^-$ pairs, as discussed in Section 6.1. The reconstructed electron or muons can be used to compute the dilepton invariant mass and it corresponds to the Z boson mass. Hence, it can be used to identify the Z boson of the signal process.

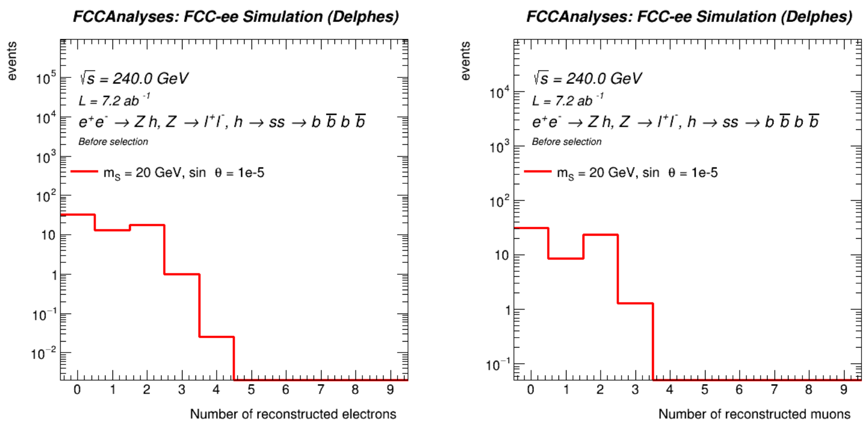

(a) Reconstructed electrons and positrons (b) Reconstructed muons

Fig. 9: Number of reconstructed electrons, positrons and muons in each event

Figure 9 shows the number of reconstructed leptons, for the signal sample with m_s = 20 GeV and $\sin\theta$ = 1e-5. The distribution for electrons and positrons is shown in Figure 9a, and it is similar to the distribution of reconstructed muons, in Figure 9b.

The peak at two is expected since the Z boson decays into two leptons. Similarly, the peak at zero corresponds to roughly 50% of the events, which is reasonable since the Z boson decays either to e^+e^- or $\mu^+\mu^-$ pairs. Hence for simulations with $Z \to \mu^+\mu^-$, there is no e^+e^- pair to be reconstructed and vice versa.

For both types, there is approximately 20% of odd number of reconstructed particles. These additional leptons most likely stem from the heavy flavour decay of the scalar. In the case when there are more than three reconstructed particles of the same kind the leptons of the same type with opposite charges and the highest momentum are used to calculate the invariant mass.

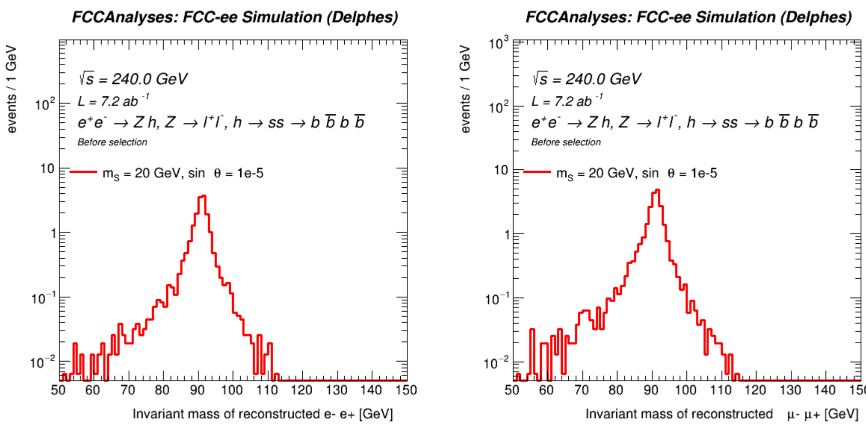

(a) From electron-positron-pairs (b) From muon-pairs

Fig. 10: Reconstructed invariant mass from the leptons.

The invariant mass of the reconstructed e^+e^- or $\mu^+\mu^-$ pairs is shown in Figure 10. It is only calculated when there are 2 or more reconstructed leptons of the same type that are oppositely charged. Both from the e^+e^- pair, see Figure 10a, and for the $\mu^+\mu^-$ pair, see Figure 10b, the invariant mass shows a peak around 91 GeV. The measured value of the Z boson mass is $m_Z = 91.1876 \pm 0.0021$ GeV, hence the Z boson mass is well reconstructed from both e^+e^- and $\mu^+\mu^-$ pairs.

7.2 Reconstructed displaced vertices

This section investigates the reconstructed DVs constructed by the procedure introduced in Section 5.5. The two routes for reconstruction, using custom track selection and custom track selection with subsequent vertex merging, are compared and analyzed for the signal samples.

7.2.1 Position of true decays and displaced vertices

Studying one event for the signal sample m_s=20 GeV, sin θ = 1e-6 Table 2 presents the positions of the true scalar decays and the DVs reconstructed using only custom track selection. The first two rows of DVs are close to but still have a displaced position compared to the first scalar, and similarly for the two last rows compared to the second scalar, indicating that these are the reconstructed DVs of the two b quarks from each scalar. Investigating another event for the same signal sample m_s=20 GeV, sin θ=1e-6 Table 3 presents the positions of the true scalar decays and the DVs reconstructed with the two different approaches, illustrating the effect of vertex merging. The first two rows of DVs in the first box, reconstructed with custom track selection, are merged together into one DV seen in the first row of the second box of DVs. Similarly, the two subsequent rows of DVs in the first box are merged together into one DV seen in the second row of the second box of DVs. This indicates that the vertex merging works well to reconstruct the DVs from each scalar. In total 7 DVs are reconstructed with custom track selection, while 5 DVs are left after vertex merging. The last three rows of DVs are possible fake vertices, reconstructed by e.g random geometric combinations.

Table 2: Example from an event with signal sample m_s=20 GeV, sin θ=1e-6 presenting the position of the vertices in x, y, z coordinates. The true positions of the two scalars are defined as MC scalars 1 and 2, and DVs are reconstructed using the custom track selection.

Vertex	x [mm]	y [mm]	z [mm]
MC scalar 1	-349.00	-22.47	-870.76
MC scalar 2	-189.32	220.82	546.42
DVs	-349.70 $\pm$ 0.106	-21.76 $\pm$ 0.040	-874.69 $\pm$ 0.415
	-349.03 $\pm$ 0.095	-23.93 $\pm$ 0.099	-873.98 $\pm$ 0.514
	-190.76 $\pm$ 0.021	221.69 $\pm$ 0.010	550.38 $\pm$ 0.040
	-190.17 $\pm$ 0.016	223.24 $\pm$ 0.069	549.43 $\pm$ 0.072

Table 3: Example from an event with signal sample m_s=20 GeV, sin θ=1e-6 presenting the position of the vertices in x, y, z coordinates. The true positions of the two scalars are defined as MC scalars 1 and 2. In the first box, DVs are reconstructed using the custom track selection, while in the second box DVs are reconstructed using custom track selection and vertex merging.

Vertex	x [mm]	y [mm]	z [mm]
MC scalar 1	8.94	8.42	6.47
MC scalar 2	-6.13	-0.63	-2.98
DVs	8.94 $\pm$ 0.018	8.41 $\pm$ 0.016	6.47 $\pm$ 0.005
with track selection	9.66 $\pm$ 0.019	8.88 $\pm$ 0.013	6.82 $\pm$ 0.008
	-5.68 $\pm$ 0.260	-0.64 $\pm$ 0.022	-2.75 $\pm$ 0.096
	-6.22 $\pm$ 0.044	-0.61 $\pm$ 0.005	-3.00 $\pm$ 0.019
	-8.27 $\pm$ 0.024	-1.60 $\pm$ 0.016	-4.75 $\pm$ 0.016
	17.40 $\pm$ 0.015	17.86 $\pm$ 0.016	14.81 $\pm$ 0.013
	16.14 $\pm$ 0.010	16.36 $\pm$ 0.010	13.48 $\pm$ 0.010
DVs	8.90 $\pm$ 0.007	8.37 $\pm$ 0.006	6.48 $\pm$ 0.003
with vertex merging	-6.17 $\pm$ 0.043	-0.61 $\pm$ 0.004	-2.97 $\pm$ 0.018
	-8.27 $\pm$ 0.024	-1.60 $\pm$ 0.016	-4.75 $\pm$ 0.016
	17.40 $\pm$ 0.015	17.86 $\pm$ 0.016	14.81 $\pm$ 0.013
	16.14 $\pm$ 0.010	16.36 $\pm$ 0.010	13.48 $\pm$ 0.010

7.2.2 Number of displaced vertices

The number of reconstructed DVs at different steps of the reconstruction procedure is shown in Figure 11 for signal sample m_s=20 GeV, sin θ=1e-6. The effect of custom track selection is seen in the figure by the shifted peak of the distributions between using no selection (red) and track selection (green and blue). Using no track selection the peak of the distribution is around 6 DVs, indicating that the reconstructed DVs are from the decay products of the b quarks. While with custom track selection, the peak of the distribution is at 4 DVs, since there are 4 true b quarks this is a good sign that the reconstruction works well. Comparing track selection with only $p_T > 1$ GeV (green) against track selection including the displaced requirement $|d_0| > 2$ mm (blue), there is no significant difference. This is expected since signal sample m_s=20 GeV, sin θ=1e-6 has a mean lifetime of roughly 1 ns, corresponding to a decay length of order 100 mm. Furthermore, when vertex merging is included the peak of the distribution is around 2, which is a good sign that the DVs correspond to the true scalar decays.

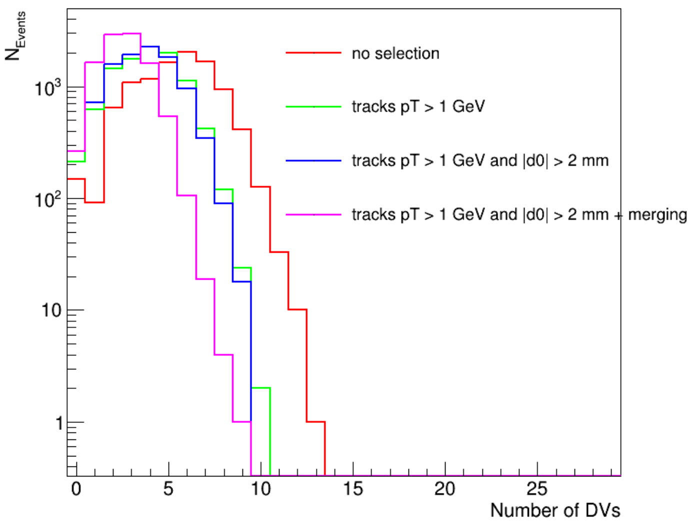

Fig. 11: The number of reconstructed DVs for signal sample m_s=20 GeV, sinθ=1e-6. The DVs are reconstructed using the secondary vertex algorithm with different criteria: all secondary tracks (red), track selection with $p_T > 1$ GeV (green), track selection with $p_T > 1$ GeV and $|d_0| > 2$ mm (blue), as well as track selection and vertex merging (purple). Note, this figure does not follow the general labeling. The y-axis is not scaled to the cross section and luminosity but shows the total number of generated events.

7.2.3 Invariant mass

To calculate the invariant mass at the DVs, the associated tracks of the DV are assigned the pion mass. Since only charged particles have tracks but a jet constitutes of both charged and neutral components, only the charged part of the jet fragmentation is captured. Hence, it is predicted to be a peak in the invariant mass distribution around half of the particle's mass [2].

In Figure 12 the invariant mass is shown for all signal samples except $m_s = 60$ GeV, $\sin\theta = $ 1e-6, the most short-lived and $m_s = 20$ GeV, $\sin\theta = $ 1e-7, the most long-lived. Comparing reconstruction with only custom track selection (12a) with reconstruction including vertex merging (12b) the heavier signal samples with $m_s = 60$ GeV (orange and purple) have distributions extended to higher values compared to the lighter signal samples (blue and red). Nevertheless, the distributions are shifted towards higher values when vertex merging is included. In Figure 12b there are no clear peaks around half of the scalar mass, which would be around 10 GeV for the red and blue distributions and around 30 GeV for the purple and orange distributions. However, there is more of a structure around these values. In Figure 12a all distributions have peaks around 1 GeV, but it is unclear if these correspond to the true b quarks or from fake vertices.

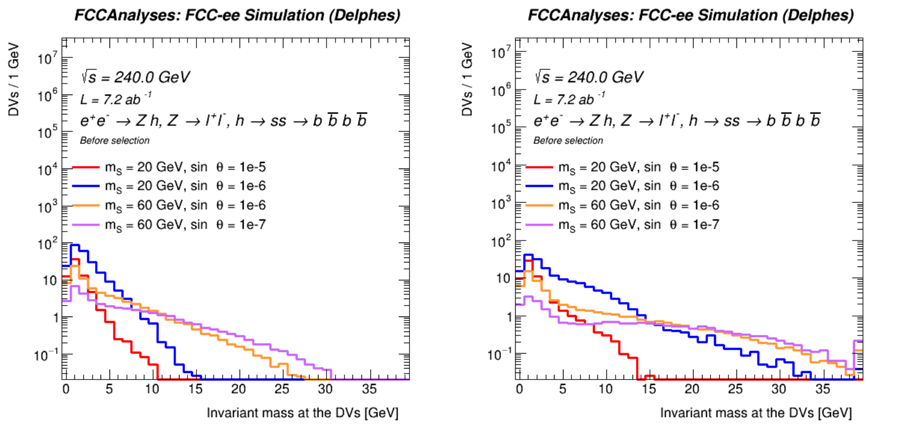

(a) Custom track selection (b) Track selection and vertex merging

Fig. 12: Invariant mass at DVs assuming all tracks to be pions.

For DV reconstruction with vertex merging, there is no step in the merging process where tracks are added to the DV after the vertex fitting is done. Therefore, tracks that could belong to a merged DV but did not pass the initial requirements or belonged to the initial vertices should be attached to a suitable DV. This would improve the accuracy of the invariant mass. Moreover, it has been mentioned in previous studies [2, 22] that for LLP masses of order tens of GeVs, it is difficult to separate the signal from the background. The background at these mass orders could stem from DVs of random geometrical crossings. A way to increase the precision for the invariant mass of the DVs and further discriminate between signal and background, which was done in [22], is to incorporate a factor regarding the geometry of the vertices. Since the tracks belonging to a true decay vertex are more likely to be collimated and facing the same direction, while for DVs of random geometrical crossings, the directions are more likely to spread out. Another suggestion which could improve the mass resolution is to include neutral hadrons and photons in the direction of the DVs.

Since the reconstructed DVs from the full procedure including vertex merging do not improve the precision of the invariant mass, it is concluded for the next step of the study to reconstruct DVs only with custom track selection.

7.2.4 Distance from primary vertex to displaced vertex

The distance between the reconstructed DVs and the PV, r_{DV-PV}, is shown in Figure 13 for all signal samples. The DVs are reconstructed using the custom track selection. Comparing Figure 13 with Figure 6 it is seen that the reconstructed lengths agree quantitatively with the generated distributions, indicating that the reconstruction procedure works well. For signal sample $m_s = 60$ GeV, $\sin\theta = $ 1e-5 (black) the number of reconstructed DVs is roughly 1% of the truth decays, indicating that the track selection with the requirement of $|d_0| > 2$ mm is too strict for the reconstructed tracks for this signal sample. The reconstructed distributions for signal samples $m_s = 20$ GeV, $\sin\theta = $ 1e-5 (red) red and $m_s = 60$ GeV, $\sin\theta = $ 1e-6 (orange) extend to larger distances compared to the generated distributions. This could imply that the DVs are reconstructed well from the displaced b quarks as intended with the custom track selection. However, the extensions of the tails are around 50-100 mm, which are large in comparison to the 0.5 mm flight distance of B hadrons, hence this is a sign of a non-negligible fake rate in the DV reconstruction.

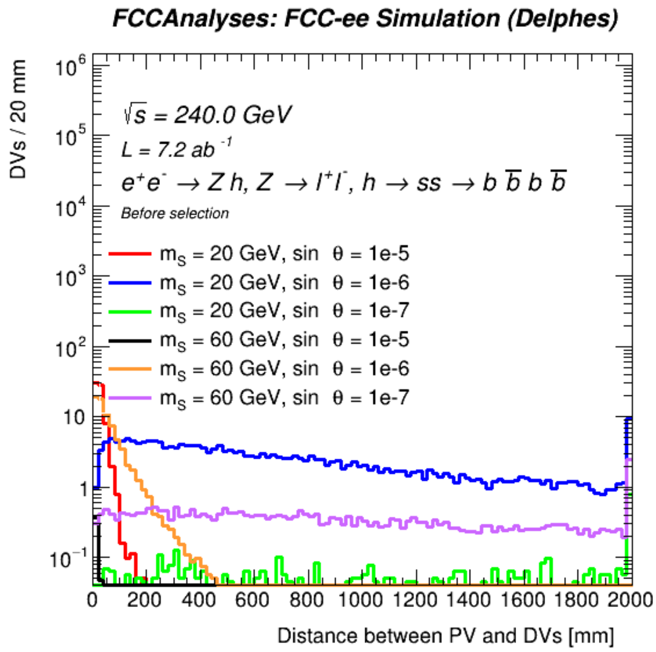

Fig. 13: The distance between the reconstructed DVs and the PV for all signal samples.

8 Sensitivity to Long-Lived Scalars from exotic Higgs decays at FCC-ee

An actual analysis of long-lived scalars from exotic Higgs boson decays needs to consider potential background processes which mimic the signals. A selection is developed in order to reduce events from the backgrounds while maintaining a large fraction of the signal event.

8.1 Background processes

The considered backgrounds include the production of WW, ZZ and Zh at $\sqrt{s}$ = 240 GeV, with inclusive decays, i.e all allowed decays according to their branching ratios. The WW production is considered to test the Z boson tagging, while the main background processes are decay channels with final states mimicking the signal process, e.g $e^-e^+ \to Zh, Z \to l^+l^-, h \to b\bar{b}, c\bar{c}$ or $\tau^+\tau^-$ and $e^-e^+ \to ZZ, Z \to l^+l^-, Z \to b\bar{b}$. The samples were generated with the same procedure as for the signal samples, centrally produced and simulated by the FCCAnalyses framework in the "spring 2021 production campaign". In this production campaign, 10^7 events were simulated for WW and Zh production, and 59.8×10^7 were simulated for ZZ production. For this study, 100.000 of the simulated events were processed for each background process.

8.2 Vertex selection

Two selection requirements are placed on the reconstructed DVs. Firstly, the distance between the reconstructed DVs and the PV, r_{DV-PV}, is required to be in the range of $4 < r_{DV-PV} < 2000$ mm. The outermost limit constrains the DVs to be within the volume of the DCH where vertices can be reconstructed. The innermost limit serves to remove vertices from heavy flavor decays that are produced promptly in the e^+e^- collision. Secondly, the charged invariant mass at the DVs, $M_{charged}$, is constrained to be higher than 1 GeV to reduce other backgrounds from fake vertices constructed by random geometrical combinations or spurious hits in the detector. As concluded in Section 7.2.3 vertex merging does not improve the reconstruction of the DVs, and hence is not applied. The full set of selections placed on the vertices, including the constraints from the reconstruction algorithm and the selection of tracks, are summarized in Table 4.

Table 4: The full set of selections placed on the vertices in this analysis

Type	Parameter	Value
Track Selection	Min p_T	1 GeV
	Min $\lvert d_0 \rvert$	2 mm
Vertex Reconstruction	V^0 rejection	True
	Max χ^2	9
	Max M_{inv}	40 GeV
	Max χ^2 added track	5
	Vertex merging	False
Vertex Selection	Min r_{DV-PV}	4 mm
	Max r_{DV-PV}	2000 mm
	Min $M_{charged}$	1 GeV

8.3 Event selection

As suggested in Section 6.1 the signal events can be tagged with the presence of a Z boson reconstructed from the invariant mass of the lepton pair. This is expected to particularly reduce the WW background. As a pre-selection, the presence of two oppositely charged electrons or muons is required, to reconstruct the invariant mass. Based on the result in Figure 10, the invariant mass of the reconstructed leptons with the highest momentum, m_{ll}, is set to be in the range from 70 to 110 GeV. This mass window range can be considered loose given the projected good lepton resolution of IDEA. However, for this particular signal the background suppresion due to a tighter mass window range would be minor compared to the requirements of the DVs. The number of DVs present in the event is the most discriminating variable between signal and background. Since the DVs are reconstructed with custom track selection, the number of DVs, n_DVs, is required to be at least two, thereby demanding at least two of the four b-quark decays to be reconstructed. All of the DVs are reconstructed according to the criteria summarized in the previous section. A summary of the event selection is presented in Table 5.

Table 5: Summary of the variables and cuts in the event selection

	Selection
Pre-selection	$\geq$ 2 oppositely charged electrons or muons
Z boson tag	$70 < m_{ll} < 110$ GeV
Multiplicity of DVs	n_DVs ≥ 2

The efficiency of each requirement applied in cumulative order on the background events is summarized in Table 6. As expected, the Z boson tag reduces the W boson pair background. Furthermore, all backgrounds are effectively reduced to zero when requiring at least two displaced vertices. The efficiencies for the signal samples are summarized in Table 7. The best efficiency is reached for the signal samples with sin θ = 1e-6, both for m_s = 20 GeV and m_s = 60 GeV, where the selection maintains 50% of the signal.

Table 6: Cut flow showing the efficiencies for each step of the event selection for the background processes. The selections are expressed to the left for each row and applied cumulatively from the top down.

	WW	ZZ	ZH
Before selection	1.0	1.0	1.0
Pre-selection	0.131	0.026	0.059
$70 < m_{ll} < 110$ GeV	0.006	0.086	0.047
n_DVs ≥ 2	0.0	0.0	0.0

8.4 Sensitivity analysis

To determine the sensitivity to the signal, the efficiencies in Tables 6 and 7 are turned into the absolute number of expected events. For this analysis the total number of signal events is given by,

$$N_{tot} = N_{Zh} \times \text{BR}(Z \to l^+l^-) \times \text{BR}(h \to ss \to b\bar{b}b\bar{b}), \quad (5)$$

with N_{Zh} being the total number of Zh events from e^+e^+ collisions at $\sqrt{s} = 240$ GeV, and the two branching ratios correspond to their respective decays. The total number of Zh events are 1.45×10^6 and the measured Z boson branching ratio to leptons is, $\text{BR}(Z \to l^+l^-) = 3.3658 \pm 0.0023\%$ where $l = e, \mu, \tau$. Hence, $\text{BR}(Z \to l^+l^-) =$

Table 7: Cut flow showing the efficiencies for each step of the event selection for the signal samples [m_s, sin θ]. The selections are expressed to the left for each row and applied cumulatively from the top down.

	20 GeV, 1e-5	20 GeV, 1e-6	20 GeV, 1e-7
Before selection	1.0	1.0	1.0
Pre-selection	0.672	0.687	0.819
$70 < m_{ll} < 110$ GeV	0.653	0.670	0.803
n_DVs ≥ 2	0.080	0.505	0.012
	60 GeV, 1e-5	60 GeV, 1e-6	60 GeV, 1e-7
Before selection	1.0	1.0	1.0
Pre-selection	0.640	0.637	0.740
$70 < m_{ll} < 110$ GeV	0.620	0.618	0.722
n_DVs ≥ 2	0.0	0.491	0.313

$2 \times 3.3658\%$ is used in Equation (5) since decays to both e and μ are considered. The full branching ratio for the Higgs can be further divided as, $\text{BR}(h \to ss \to b\bar{b}b\bar{b}) = \text{BR}(h \to ss) \times \text{BR}(s \to b\bar{b})^2$, with,

$$\text{BR}(h \to ss) = \frac{\Gamma(h \to ss)}{\Gamma_h} = \frac{\kappa^2 v_h^2}{32\pi m_h \Gamma_h}\sqrt{1 - 4\frac{m_s^2}{m_h^2}}. \tag{6}$$

Here, $\Gamma_h = \Gamma_h^{SM} + \Gamma(h \to ss)$ with $\Gamma_h^{SM} = 0.0032$ GeV and $m_h = 125$ GeV, $v_h = 246$ GeV, $\kappa = 7\text{e-}4$ and $m_s = 20$ or 60 GeV, and BR $(s \to b\bar{b})^2 = 0.9^2$, seen in the left plot of Figure 1.

The resulting total number of events for each signal sample is summarized in Table 8 together with the calculated $\text{BR}(h \to ss)$ and the number of expected events. To compare with the selection placed on the distance for the reconstructed DVs, the last column presents the number of events where at least one of the scalars has a decay length within the range of 4-2000 mm. The lower bound of this constraint reduces the sensitivity of the signal sample $m_s = 60$ GeV, sin θ = 1e-5. While the signal sample $m_s = 20$ GeV, sin θ = 1e-7 is too long-lived and hence limited by the DCH volume.

Additionally, the calculated number of events can be used for computations at the reconstruction level. Table 10 summarizes the number of signal events, and Table 9 the number of background events, before and after each event selection. The number of events N is normalized according to,

$$N = \frac{N_{tot}}{N_{gen}^{tot}} N_{gen}^{cut},$$

where N_{tot} is the total number of signal events as given in Equation 5, N_{gen}^{tot} is the total number of generated events and N_{gen}^{cut} the number of generated events after each

Table 8: The calculated mean proper lifetime $c\tau$, $\mathrm{BR}(h \rightarrow ss)$, the total expected events and expected selected events where at least one of the scalars has a decay length $4 < L_{xyz} < 2000$ mm, for all generated scalar masses m_S and mixing angles $\sin\theta$.

Mass of Scalar m_S [GeV]	Mixing angle $\sin\theta$	Mean proper lifetime $c\tau$ [mm]	Branching Ratio $\mathrm{BR}(h \rightarrow ss)$	Total expected events	Expected selected events
20	1×10^{-5}	3.4	6.98×10^{-4}	55.20	49.88
20	1×10^{-6}	341.7	6.98×10^{-4}	55.20	53.91
20	1×10^{-7}	34167.0	6.98×10^{-4}	55.20	1.96
60	1×10^{-5}	0.9	2.06×10^{-4}	18.85	0.02
60	1×10^{-6}	87.7	2.06×10^{-4}	18.85	16.18
60	1×10^{-7}	8769.1	2.06×10^{-4}	18.85	10.72

applied cut. The statistical uncertainty σ_{error} is given by,

$$\sigma_{error} = \frac{N_{tot}}{N^{tot}_{gen}} \sqrt{N^{cut}_{gen}}.$$

Table 9: Number of events for each considered background, before and after each cut. The uncertainties are statistical.

	Before selection	Pre-selection	$70 < m_{ll} < 110$ GeV	n_DVs ≥ 2
WW	1.18e+08 $\pm$ 1.29e+07	3.04e+06 $\pm$ 5.99e+04	6.73e+05 $\pm$ 2.82e+04	0 ($\leq$ 2.82e+04)
ZZ	9.78e+06 $\pm$ 3.06e+05	1.28e+06 $\pm$ 1.12e+04	8.43e+05 $\pm$ 9.08e+03	0 ($\leq$ 9.08e+03)
ZH	1.45e+06 $\pm$ 1.75e+04	8.60e+04 $\pm$ 1.12e+03	6.84e+04 $\pm$ 9.97e+02	0 ($\leq$ 9.97e+02)

Table 10: Normalized number of events for each signal sample, before and after each cut. The uncertainties are statistical.

m_s, sin θ	Before selection	Pre-selection	$70 < m_{ll} < 110$ GeV	n_DVs ≥ 2
20 GeV, 1e-5	55.2 $\pm$ 0.0413	37.3 $\pm$ 0.455	36.2 $\pm$ 0.448	4.45 $\pm$ 0.157
20 GeV, 1e-6	55.2 $\pm$ 0.0413	38.1 $\pm$ 0.460	37.2 $\pm$ 0.454	28.0 $\pm$ 0.394
20 GeV, 1e-7	55.2 $\pm$ 0.0413	45.4 $\pm$ 0.502	44.5 $\pm$ 0.497	0.665 $\pm$ 0.0607
60 GeV, 1e-5	18.9 $\pm$ 0.00813	12.0 $\pm$ 0.150	11.6 $\pm$ 0.148	0 ($\leq$ 0.148)
60 GeV, 1e-6	18.9 $\pm$ 0.00813	12.0 $\pm$ 0.150	11.6 $\pm$ 0.147	9.21 $\pm$ 0.131
60 GeV, 1e-7	18.9 $\pm$ 0.00813	13.9 $\pm$ 0.161	13.5 $\pm$ 0.159	5.87 $\pm$ 0.105

To determine to which extent the FCC-ee will be sensitive to the long-lived scalars, given these signal signatures, the exclusion reach is set with the upper limit CL 95%. Based on a zero background, a signal can be excluded to CL 95% if the expected number of events is at least 3. In Table 9 the number of events from each background process is shown, after the final cut there are 0 expected events. The uncertainties which are reduced to roughly 1% are expected to be further reduced if all the generated events in the spring2021 production campaign are considered. In Table 10 the number of events for all signal samples is shown. All signal samples but $m_s = 20$ GeV, sin θ = 1e-7 and $m_s = 60$ GeV, sin θ = 1e-5 have at least 3 events left after the full event selection and thereby possibilities to be within reach for the FCC-ee. This is in line with the truth level sensitivity analysis shown in the last column of Table 8. Since the BR($h \to ss$) is of order 10^{-4}, see Table 8, the possible exclusion limits set at the FCC-ee are more sensitive than current limits, see Section 2.2. The highest sensitivity is achieved for the signal sample with $m_s = 20$ GeV, sin θ = 1e-6, i.e for lifetimes of approximately 0.3 m. This is expected since the majority of the scalars would decay inside the DCH but have a decay length sufficiently long to pass the displacement requirements.

A crucial factor not yet considered in this sensitivity analysis is the reconstruction efficiency of the vertices, i.e how often a reconstructed DV actually corresponds to any of the long-lived scalar decays. A scalar decay can be considered reconstructed if the tracks associated with a DV are matched to any of the truth particle b quarks originating from the scalar. Hence, truth matching needs to be performed to measure the fraction of true reconstructed DVs compared to miss-reconstructed DVs.

Finally, it is necessary to repeat the approximations done in this study to see under which assumptions these results hold. The long-lived scalar is simulated by explicitly setting the decay width of the scalar in the `MadGraph` process card. This decay width is calculated from leading order expressions of the partial decay width of $\Gamma(s \to b\bar{b})$ together with the branching ratio of this decay taken from the plot in Figure 1. A higher precision of these variables could modify the determined sensitivity. Therefore, it is desirable to repeat the study with a more consistent framework for a more reliable result.

9 Outlook

Two suggestions for the continuation of this work have been introduced. Firstly, to improve the vertex merging by adding tracks to the DV which do not belong to the initial vertices but are associated with the merged DV, to improve the reconstruction procedure and possibly the precision of the invariant mass at the DVs. Secondly, a redo of this study with another `MadGraph` model, preferably constructed only for the model with an extension of the SM with a scalar, is desirable.

Another suggestion is to generate more signal samples with different masses and lifetimes, to properly span the full parameter space for this signal signature. Suggested ranges for a grid search are m_s = 10, 20, 30, 40, 50, and 60 GeV and with mean proper lifetime in the span of 3-2000 mm, i.e $\sin\theta = 10^{-5}, 10^{-6}$ and 10^{-7}. Also, since the main background in LLP searches with a DV signature is more likely to stem from sources like interactions of particles with the detector material, a full detector simulation could be considered for future analyses.

Furthermore, the jets in the signal events are advised to be analyzed to study possible discriminating variables to include in the event selection. The implemented SV finder can be used to find SV within jets. Hence, an alternative DV reconstruction procedure is to identify the DVs corresponding to each b quark within the jets. Another interesting LLP signature to consider for jet studies is delayed jets, where the jet timing is important to investigate.

At last, an investigation of alternative experimental signatures, such as a hadronic decay of the Z boson would be interesting to conduct. Since the FCC-ee offers a clean background all hadrons in an event should belong in a jet. If the dijet stemming from the Z boson can be distinguished from the LLP jets and backgrounds, the total production cross section for the signal process would potentially increase with a magnitude of 10, due to the higher branching ratio.

10 Conclusion

This note aimed to investigate the sensitivity of exotic Higgs decays to long-lived scalars at FCC-ee. All the work was done within the FCCAnalyses framework, where simulations were generated using `MadGraph`, PYTHIA, and DELPHES. The model considered for signal interpretations was the scalar extension of the SM. To generate signal simulations the HAHM `MadGraph` model was used, where the dark photon is decoupled to only consider the phenomenology of the scalar. The relevant stage of the FCC-ee is the Zh stage with $\sqrt{s} = 240$ GeV. The pair production and decay of the scalars studied in this note include a hadronic final state with a $b\bar{b}$ pair from each scalar. Furthermore, the Z boson was restricted to a leptonic decay. The parameter space was defined for two scalar masses $m_s = 20$ and 60 GeV and three mixing angles $\sin\theta = 10^{-5}, 10^{-6}$ and 10^{-7}, corresponding to decay lengths of order 1 mm to 10 m. Addtionally, the Higgs-scalar coupling κ was set to $\kappa = 7\times10^{-4}$, such that BR$(h \to ss)$ is of order 10^{-4}. Kinematics of the scalar, such as the decay length and lifetime, was studied and validated compared to theoretical predictions for all signal samples.

To reconstruct the DVs from the long-lived scalar, this note utilized the FCC-Analyses version of the secondary vertex algorithm LCFIPlus, extended with a track selection. Moreover, vertex merging was also implemented but not included in the vertex selection and sensitivity analysis. To study the sensitivity, an event selection was proposed based on identifying the Z boson from the invariant mass of two oppositely charged leptons and the presence of at least two DVs. The event selection effectively reduced the considered background processes of the W boson pair -, the Z boson pair-, and the Z and Higgs boson pair production, to zero. To compute the number of expected events for the signal samples, the cross section was approximated from the total production cross section of the Z boson and the Higgs boson multiplied by the relevant branching ratios. Within this limitation, all signal samples, except $m_s = 20$ GeV, sinθ = 1e-7 and $m_s = 60$ GeV, sinθ = 1e-5, have 3 or more expected events after the event selection. This indicates that the FCC-ee has the possibility to set a lower exclusion limit on the BR$(h \to ss)$ than current limits. The highest sensitivity is achieved for lifetimes of approximately 0.3 m.

References

[1] D. Curtin, R. Essig, S. Gori, P. Jaiswal, A. Katz, T. Liu, Z. Liu, D. McKeen, J. Shelton, M. Strassler, Z. Surujon, B. Tweedie, Y.M. Zhong, Exotic decays of the 125 GeV Higgs boson. Physical Review D **90**(7), 075004 (2014). https://doi.org/10.1103/PhysRevD.90.075004. Publisher: American Physical Society

[2] J. Alimena, J. Beacham, et al, Searching for long-lived particles beyond the Standard Model at the Large Hadron Collider. Journal of Physics G: Nuclear and Particle Physics **47**(9), 090501 (2020). https://doi.org/10.1088/1361-6471/ab4574. Publisher: IOP Publishing

[3] M. Vande Voorde, Long-Lived Particles from exotic Higgs decays at the FCC-ee. Master thesis, Uppsala University (2023). URL https://uu.diva-portal.org/

smash/record.jsf?pid=diva2:1742588

[4] M.J. Strassler, K.M. Zurek, Echoes of a hidden valley at hadron colliders. Physics Letters B **651**(5), 374–379 (2007). https://doi.org/10.1016/j.physletb.2007.06.055

[5] N. Craig, A. Katz, M. Strassler, R. Sundrum, Naturalness in the dark at the LHC. Journal of High Energy Physics **2015**(7), 105 (2015). https://doi.org/10.1007/JHEP07(2015)105

[6] G. Krnjaic, Probing light thermal dark matter with a Higgs portal mediator. Physical Review D **94**(7), 073009 (2016). https://doi.org/10.1103/PhysRevD.94.073009. Publisher: American Physical Society

[7] M. Cepeda, S. Gori, V.I. Martinez Outschoorn, J. Shelton, Exotic Higgs Decays. Annual Review of Nuclear and Particle Science **72**(1), 119–149 (2022). https://doi.org/10.1146/annurev-nucl-102319-024147

[8] S. Alipour-fard, N. Craig, M. Jiang, S. Koren, Long live the Higgs factory: Higgs decays to long-lived particles at future lepton colliders *. Chinese Physics C **43**(5), 053101 (2019). https://doi.org/10.1088/1674-1137/43/5/053101

[9] A. Abada, M. Abbrescia, et al, FCC-ee: The Lepton Collider. The European Physical Journal Special Topics **228**(2), 261–623 (2019). https://doi.org/10.1140/epjst/e2019-900045-4

[10] H. Jarlett, The Future Circular Collider (2016). URL https://cds.cern.ch/record/2138983

[11] G. Bernardi, E. Brost, et al. The Future Circular Collider: a Summary for the US 2021 Snowmass Process (2022). https://doi.org/10.48550/arXiv.2203.06520

[12] F. Bedeschi, in *Proceedings of 40th International Conference on High Energy physics — PoS(ICHEP2020)*, vol. 390 (SISSA Medialab, 2021), p. 819. https://doi.org/10.22323/1.390.0819. URL https://pos.sissa.it/390/819

[13] N. Bacchetta, J.J. Blaising, et al. CLD – A Detector Concept for the FCC-ee (2019). https://doi.org/10.48550/arXiv.1911.12230

[14] P. Giacomelli. The idea detector concept (2022). URL https://indico.cern.ch/event/1064327/contributions/4888532/

[15] J. Alwall, R. Frederix, S. Frixione, V. Hirschi, F. Maltoni, O. Mattelaer, H.S. Shao, T. Stelzer, P. Torrielli, M. Zaro, The automated computation of tree-level and next-to-leading order differential cross sections, and their matching to parton shower simulations. Journal of High Energy Physics **2014**(7), 79 (2014). https://doi.org/10.1007/JHEP07(2014)079

[16] C. Bierlich, S. Chakraborty, N. Desai, L. Gellersen, I. Helenius, P. Ilten, L. Lönnblad, S. Mrenna, S. Prestel, C.T. Preuss, T. Sjöstrand, P. Skands, M. Utheim, R. Verheyen. A comprehensive guide to the physics and usage of PYTHIA 8.3 (2022). https://doi.org/10.48550/arXiv.2203.11601

[17] S. Ovyn, X. Rouby, V. Lemaitre. Delphes, a framework for fast simulation of a generic collider experiment (2010). https://doi.org/10.48550/arXiv.0903.2225

[18] A. Blondel, P. Janot. FCC-ee overview: new opportunities create new challenges (2021). https://doi.org/10.48550/arXiv.2106.13885

[19] T. Suehara, T. Tanabe, LCFIPlus: A framework for jet analysis in linear collider studies. Nuclear Instruments and Methods in Physics Research Section A: Accelerators, Spectrometers, Detectors and Associated Equipment **808**, 109–116 (2016). https://doi.org/10.1016/j.nima.2015.11.054

[20] Performance of vertex reconstruction algorithms for detection of new long-lived particle decays within the ATLAS inner detector (2019)

[21] D. Curtin, R. Essig, S. Gori, J. Shelton, Illuminating dark photons with high-energy colliders. Journal of High Energy Physics **2015**(2) (2015). https://doi.org/10.1007/jhep02(2015)157

[22] J. Burzynski, A Search for Exotic Higgs Decays or: How I Learned to Stop Worrying and Love Long-lived Particles". Ph.D. thesis, Simon Fraser University (CA) (2021). URL https://cds.cern.ch/record/2780737